Journal of Nuclear Materials 405 (2010) 59–69

Contents lists available at ScienceDirect

Journal of Nuclear Materials

journal homepage: www.elsevier.com/locate/jnucmat

A study on martensitic phase transformation in 9Cr–1W–0.23V–0.063Ta–0.56Mn–0.09C–0.02N (wt.%) reduced activation steel using differential scanning calorimetry

S. Raju [a,*], B. Jeya Ganesh [a], Arun Kumar Rai [a], R. Mythili [a], S. Saroja [a], Baldev Raj [a,b]

[a] Physical Metallurgy Division, Metallurgy and Materials Group (IGCAR), Kalpakkam 603102, India
[b] Indira Gandhi Centre for Atomic Research (IGCAR), Kalpakkam 603102, India

ARTICLE INFO

Article history:
Received 23 November 2009
Accepted 23 July 2010

ABSTRACT

The salient characteristics of martensite formation kinetics in 9Cr–1W–0.23V–0.063Ta–0.09C–0.02N (wt.%) reduced activation steel have been investigated using differential scanning calorimetry and supplemented by microscopy characterisation. Accurate determination of the martensite start (M_S) and finish (M_f) temperatures as a function of cooling rate (1–99 K min^{-1}) and holding time (1–120 min) in the γ-austenite phase field have been made. The critical cooling rate to form nearly 100% martensite is found to be of the order of 5–6 K min^{-1}. The measured latent heat for the martensite transformation is found to be in the range 62–75 J g^{-1}. In the case of austenitisation at 1323 K, it is found that the grain size of the parent austenite exhibited significant growth and the observed M_S temperature too exhibited a systematic increase with austenite grain size. However, for those samples that are solution treated at a slightly lower temperature of 1253 K, the M_S is found to be initially insensitive to the increase in holding time for up to about 30 min. This trend is followed later on by the usual increasing character of M_S for further rise in the holding periods, up to about 120 min. This unusual initial behaviour is also reflected by the corresponding variation in the hardness values of the quenched in martensite. Moreover, the growth of parent austenite grains has also been restricted during the initial phase of solution annealing at 1253 K. This is attributed to the presence of undissolved carbide particles, which exert a pinning influence on the movement of austenite grain boundaries. The observed athermal martensite formation kinetics is described well by the Koistinen–Marburger relation.

1. Introduction

A study of martensite formation in high chromium ferritic steels is of interest in both scientific and technological perspectives. The formation of hard and brittle martensite as a result of the solutionising and quenching heat treatment and its subsequent tempering to achieve the desired balance between toughness and strength constitute the core physical metallurgy of modern power plant steels [1–10]. Not surprisingly therefore, numerous studies, both on experimental [11–48] and modelling – simulation fronts [49–84] have been conducted till date to understand the phase and microstructural stability of these alloys upon high temperature service-exposure and the attending changes in physical and mechanical properties in terms of simple intuitively understood metallurgical concepts. Thanks to the immense and coordinated worldwide research, the present day high chromium power plant steels have scientifically tailored chemical compositions, melting practices and thermomechanical processing schedules that make possible the attainment of fairly stable microstructure with desired physical and mechanical properties [1,2].

Admittedly, the bulk of the current characterisation research on modern 9Cr-based ferritic steels are at the interface of physical, mechanical and process metallurgy, with relatively few of these investigations devoted exclusively to probing the fundamental thermodynamic and kinetic aspects of phase stability [10,26,49,50,52–56,58]. It is needless to stress the fact that a fundamental study on thermodynamics and kinetic considerations of phase stability is indeed germane to evolving a strategically transparent approach to alloy design [85]. It is amidst this background that we have undertaken in our recent study on the indigenously developed reduced activation ferritic–martensitic (RAFM) steel, a comprehensive calorimetry characterisation of various on-heating diffusional phase transformations up to melting [86]. Owing to reasons of restricted scope, this earlier report did not include details of the diffusionless martensitic transformations that follow as a result of cooling from the high temperature γ-austenite phase field. A comprehensive understanding of the

* Corresponding author. Tel.: +91 44 274 80 306; fax: +91 44 274 80 081.
E-mail address: sraju@igcar.gov.in (S. Raju).

0022-3115/$ - see front matter © 2010 Elsevier B.V. All rights reserved.
doi:10.1016/j.jnucmat.2010.07.036

martensite formation characteristics, especially its kinetics as a function of process parameters like time and temperature of austenitisation and cooling rate from the austenite phase field is rather essential from the point of view of arriving at the optimal solutionising treatment conditions [17]. It is the purpose of the present study to address the basic kinetic aspects of martensite formation in a typical 9Cr-based RAFM steel using dynamic calorimetry technique.

2. Experimental details

The reduced activation ferritic–martensitic (RAFM) steel used in the present study belongs to the same heat from which samples for our previous study were drawn [86]. Its chemical composition as determined by X-ray fluorescence spectroscopy is listed in Table 1. The presence of about 1 wt.% W, 0.63 wt.% Ta, 0.2 wt.% V with about 0.09 wt.% C and 0.02 wt.% N is rather noteworthy. In a similar vein, the near absence of certain transition elements like Nb, Mo, Ti, in addition to certain non-transition solutes like Si, Cu and Al deserves special mention as these are known to produce long lived radioactive isotopes under the influence of high energy neutrons [87]. The details regarding melting and other ingot processing practices have already been briefed in our earlier report [86]. For the present study however, small sections of varying dimensions have been cut from the as supplied ~25 mm thick hot forged plates and from these pieces, small approximately about $2 \times 2 \times 2$ mm cubes were sliced using diamond coated slow speed wire saw. These regularly shaped small cubes after adequate cleaning in alcohol were accurately weighed in a microbalance to ±0.1 mg accuracy. These served as the starting samples for our subsequent controlled cooling studies carried out *in situ* in the heat-flux type *Setaram Setsys 16* DSC apparatus. Since, the basic details of the DSC experiments have already been elaborated upon in our previous publications [26,86], these are not described here. However, it is instructive to reiterate certain salient features of the current experiments.

All the DSC runs were carried out with fresh samples in high pure (Iolar grade 2) flowing argon (50 ml per min) atmosphere. The Fe-80 mass *ppm* C alloy (Aldrich Chemicals) was used as the temperature and heat flow calibrant. The precision of temperature measurement is estimated to be ±2 K in 673–1373 K region. The cooling rates employed were varied from 1 to 100 K min^{-1} and the soaking time in the γ-austenite phase field was varied from 1 to 120 min with about 10 discrete unequal time steps.

2.1. Experimental plan

Since the present study aims at characterising the athermal martensite formation upon controlled cooling, the following experimental plan is adopted. The starting microstructure for all our experiments is obtained by solutionising the steel at 1253 K for 15 min, followed by aircooling to room temperature. Subsequent tempering at 1033 K for about 30 min is carried out in air. The choice of 1253 K as the solutionising temperature is quite typical of the normalising practice adopted in the case of similar high chromium reduced activation steels, such as Eurofer [88].

In one set of experiments, the normalised and tempered (N&T) samples are heated inside the DSC cell at a fixed rate of 10 K min^{-1} under flowing high pure argon atmosphere to the required solutionising temperature in γ-austenite regime. The samples are kept for different time periods, in the range 1–120 min at this temperature. At the end of this isothermal holding session, the samples were cooled to room temperature at a constant rate of 99 K min^{-1}. This set of experiments has been designed to monitor the effect of holding time in the austenite region on martensite transformation characteristics under constant cooling rate. In the present study, we have selected two solutionising temperatures in the γ-austenite region, namely 1253 and 1323 K respectively. It is found that prolonged exposures at temperatures exceeding about 1373 K resulted in some δ-ferrite formation [86] and it is desired to avoid the formation of this phase, as this will complicate the straight forward interpretation of the major factors that influence the martensite formation kinetics [89].

In the second set of experiments designed to estimate the critical cooling rate needed for producing martensite, an array of samples were austenitised at a fixed temperature of 1253 K for a fixed time of about 15 min. These samples were subsequently cooled to room temperature at different rates ranging from 1 to 99 K min^{-1}. Further, the quenched in microstructure of these samples were also characterised by metallography and hardness measurements to assess the extent of martensite formation under different cooling conditions. For metallography studies, the specimens were ground and polished in the standard manner and for revealing the prior austenite grain boundaries, a mild initial etch with 2% nital, followed by another using Villella's reagent was carried out. The light microscopy observations were made using *Leica* MeF4A optical microscope equipped with digital image acquisition. The microhardness measurements were carried out in a *Leitz* microhardness tester using 100 g load. In general, about eight to ten hardness measurements were made and the average value is reported here. Samples for thin foil transmission electron microscopy study were obtained by the ion milling technique. The electron microscopy observations were made in a Philips CM 20® microscope operating at 200 keV. In the following section, the major experimental results are presented in a systematic fashion.

3. Results

3.1. Basic microstructure

In Fig. 1a, the typical optical micrograph corresponding to 1253 K/15 min normalised microstructure is portrayed. The presence of nicely outlined prior austenite grain boundaries enclosing packets of lath martensite is immediately apparent. In addition, it is also evident that some undissolved carbide particles are still present after 1253 K/15 min normalisation treatment. However, their volume fraction is expected to be small as compared to tempered condition. In Fig. 1b, the transmission electron micrograph illustrates the typical dislocation ridden morphology of lath martensite and the stray presence of undissolved carbide particle, marked by arrow. In Fig. 1c, the effect of tempering at 1033 K for 30 min is illustrated. Copious amount of small carbide precipitates are seen to decorate prior austenite, interlath and intercolony boundaries of the tempered martensite matrix. The microhardness measurements revealed that the martensite produced after the normalising treatment possessed a hardness value, in the range 425–435 VHN, and following tempering at 1033 K for 30 min, the hardness tapered down to 250 VHN. These values are in expected order for the generic 9Cr-based steels [90].

Table 1
The chemical composition in weight percent of the reduced activation steel used in this study.

Element	C	Cr	Mo	Mn	Si	V	Al	Ni	P	Co	Cu	S	N	W	Ti	Nb	Ta
wt.%	0.091	9.05	0.0036	0.56	0.05	0.226	0.0036	–	–	0.0043	0.005	–	0.0206	1.0	0.0024	0.0039	0.063

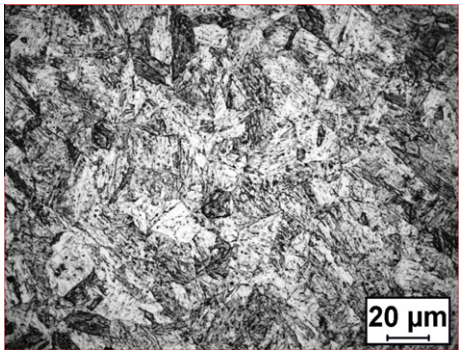

Fig. 1a. The optical micrograph of the 1253 K/15 min normalised sample showing packets of lath martensite and well delineated prior austenite grain boundaries.

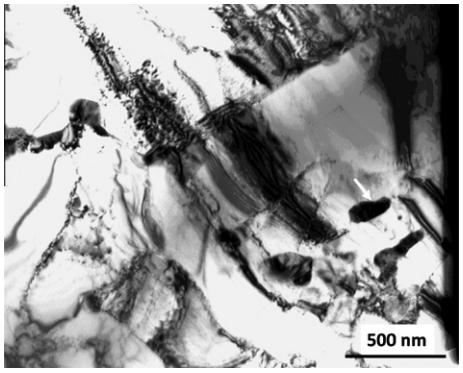

Fig. 1b. The bright field TEM micrograph of the 1253 K/15 min normalised sample showing lath martensite and a carbide particle marked by arrow.

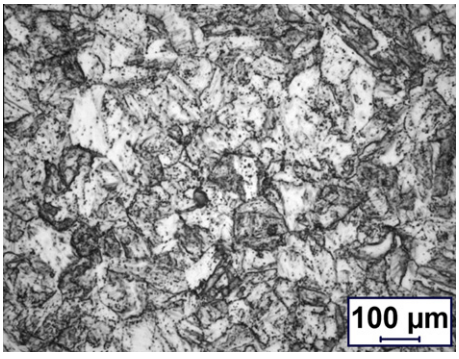

Fig. 1c. The optical micrograph showing the effect of tempering at 1033 K for 30 min.

3.2. DSC results of martensitic transformation: critical cooling rate determination

In Fig. 2, a typical DSC profile obtained during heating of the normalised and tempered sample to 1253 K and cooling thereupon at 30 K min^{-1} after 15 min hold, is illustrated. Apart from two distinct endothermic on-heating transformation peaks which arise respectively from the magnetic and α-ferrite + carbide → γ-austenite, phase changes [26,86], the presence of a *dominant exothermic* peak in the cooling cycle due to γ-austenite → α′-martensite formation is also clearly evident. The on-cooling transformation onset and offset temperatures, normally designated as the martensite start (M_S) and finish (M_f) temperatures have also been clearly marked in Fig. 2. In addition, it should also be noticed that

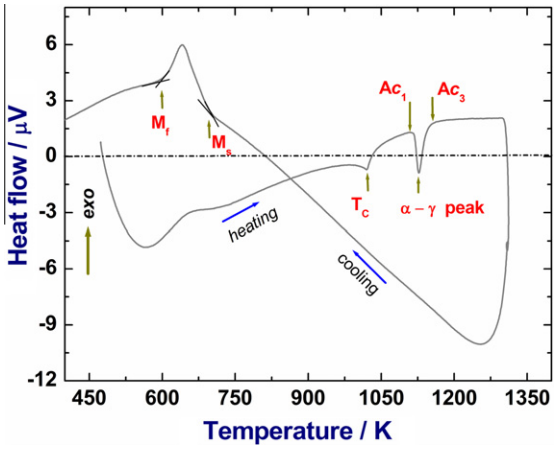

Fig. 2. The DSC profile recorded at 30 K min^{-1} scan rate, showing clearly marked endothermic and exothermic transformation arrests during heating and cooling cycles respectively.

the area enclosed by the martensite transformation peak and hence the net martensite transformation enthalpy ($\Delta^{\circ}H^{\gamma\rightarrow\alpha'}$) is considerably larger than the corresponding value ($\Delta^{\circ}H^{\alpha'\rightarrow\gamma}$) obtained for its on-heating diffusional counterpart, namely α-ferrite + carbide → γ-austenite, transformation.

Since it is well known that the ease of martensite formation depends sensitively on the cooling rate [17], a set of different cooling rates in the range 1–99 K min^{-1} was imposed on different, but closely identical samples to determine the critical cooling rate that is necessary to obtain nearly 100 percent martensite. In Figs. 3a and 3b, the peak profiles representing martensite formation that were obtained during cooling from 1253 K at different rates have been presented. Incidentally, it must be mentioned that for very slow cooling of less than about 3 K min^{-1}, no discernible exothermic peak due to martensite transformation is obtained in the present study. Moreover, it is also interesting to note that although a shallow exothermic peak is observed for some moderate cooling rates, such as 3–5 K min^{-1} (Fig. 3a), the quantum of martensite formed in these cases is rather meagre. With this background information, it is clearly seen from the nature of the peak profiles shown in Fig. 3a that the area of the transformation peak shows a gradual increase with increasing cooling rate in the low cooling rate regime, and this attains saturation only at about 40 K min^{-1} (Fig. 3b). This

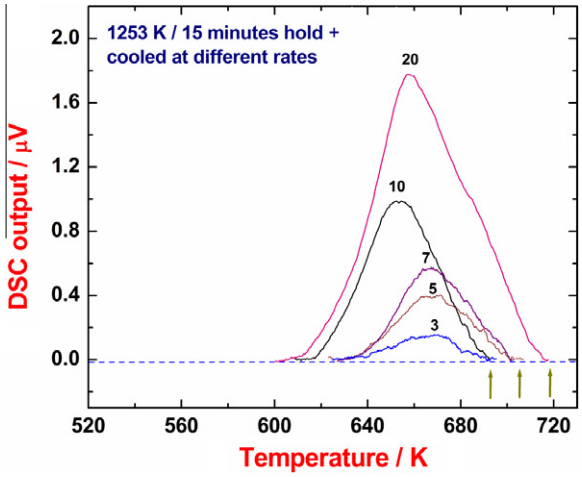

Fig. 3a. The collage of exothermic transformation peak profiles obtained for lower range of cooling rates. The austenitising conditions are 1253 K/15 min.

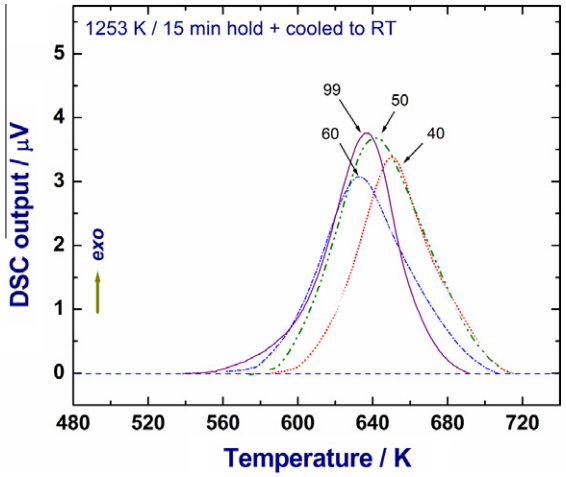

Fig. 3b. Same as Fig. 3a with peak profiles obtained for higher range of cooling rates.

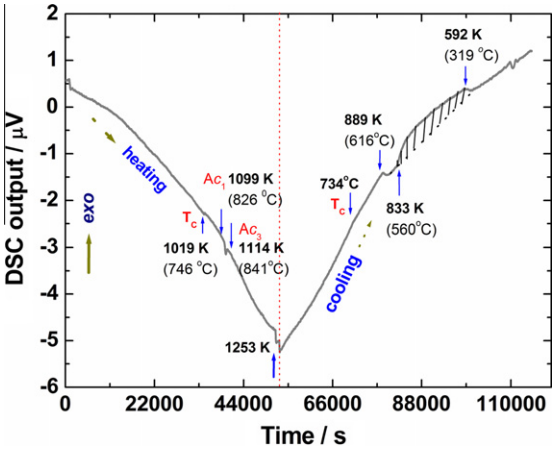

Fig. 5. The DSC profile pertaining to 1 K min^{-1} cooling rate. Note the absence of the highly exothermic martensitic transformation peak.

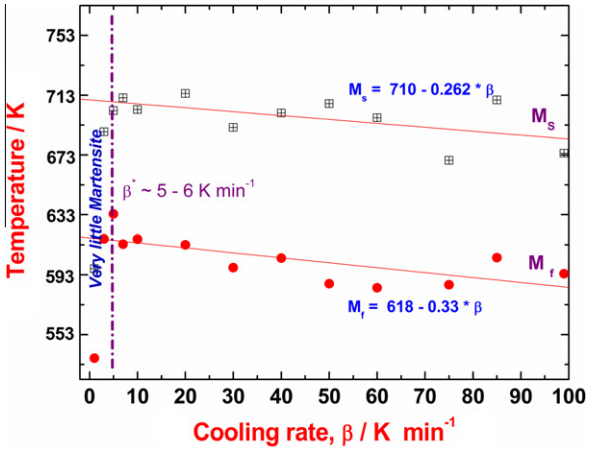

Fig. 4. Variation of M_S and M_f temperatures with cooling rate for 1253 K solution annealed samples.

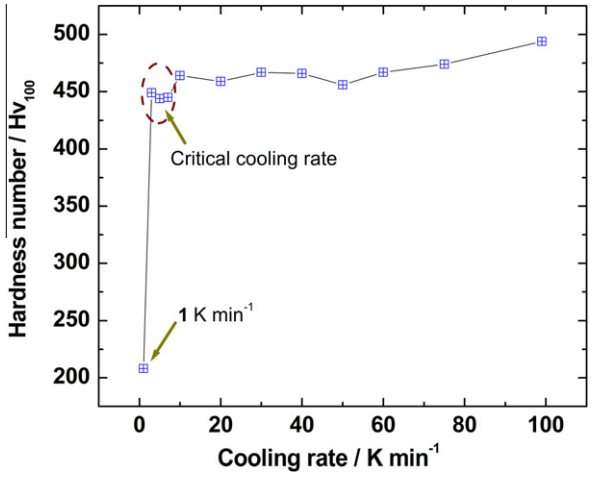

Fig. 6. The variation of microhardness of with cooling rate. Note the sudden increase in the hardness values at the critical cooling rate due to martensite formation.

indicates that in the low to moderate cooling rate regime, the extent of total martensite formed exhibits an increase with cooling rate. In Fig. 4, the measured sensitivity of M_S and M_f temperatures to increasing cooling rate is graphically portrayed. It may be seen that notwithstanding the scatter in the transformation temperature data which is generally the case with martensitic transformation in high chromium ferritic steels [90], a small decrease in martensite start (M_S) and finish (M_f) temperatures with increasing cooling rate is readily apparent [26]. But the important point to observe here is that for low cooling rates less than about 3 K min^{-1}, the measured onset transformation point does not correspond to the martensite product, but instead to the $M_{23}C_6$ carbide precipitation in α-ferrite matrix. This latter fact is clearly inferred from the cooling cycle DSC profile recorded for 1 K min^{-1} and this is displayed in Fig. 5. In this figure, the broad exothermic trough that is, the hatched area seen after ferrite formation at 833 K corresponds to the continuous carbide precipitation event. In the present set of experiment, the carbide precipitation is seen to persist right down to 592 K.

Reverting our attention back to martensite formation during controlled cooling, we may say that it is only in excess of the critical cooling rate of about 5 or 6 K min^{-1} the onset of a true martensite transformation peak becomes distinctly evident in our DSC study. This fact is even more dramatically displayed in Fig. 6, wherein the microhardness values of the martensite product are plotted against the corresponding cooling rate. The lower bound value of the hardness noted in the 1–3 K min^{-1} region corresponds to the α-ferrite phase formed out of diffusional decomposition of γ-austenite. It is only above the 5–6 K min^{-1} threshold, the formation of martensite upon cooling is clearly attested by the pronounced increase in hardness. As a brief passing remark, it may also be added that the metallographic inspection of 1 K min^{-1} cooled sample revealed only α-ferrite + carbide constituents [90]. In deference to brevity, this microstructural evidence is not presented here.

3.3. Effect of holding time and temperature in the γ-austenite region on martensite formation

In Figs. 7a and 7b the DSC peak profiles obtained, when the RAFM steel is cooled from 1253 K at 99 K min^{-1}, after different periods of isothermal hold are grouped together. From Fig. 7a, it appears that for holding time up to about 15 min at 1253 K, the M_S and M_f temperatures are not significantly altered. However, the longer durations of isothermal hold, up to about 120 min produce considerable shift in M_S temperature; in fact the M_S temperature is found to increase with the austenitising time. As a

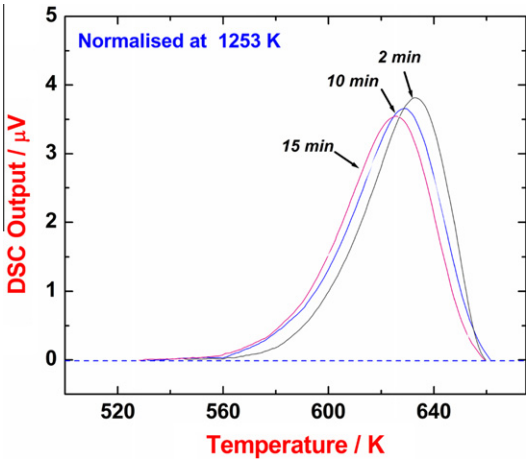

Fig. 7a. A collage of DSC peak profiles obtained during cooling at 99 K min^{-1} after different periods of holding at 1253 K.

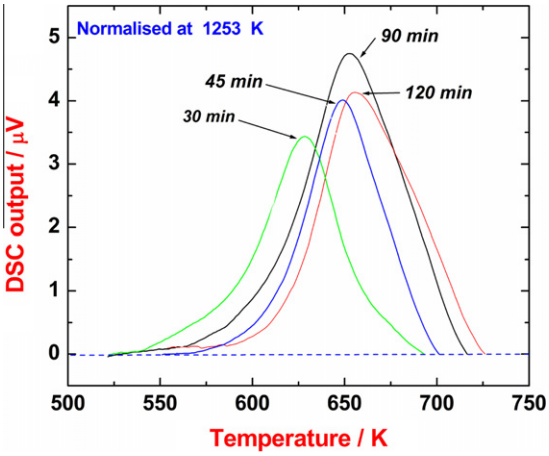

Fig. 7b. Same as Fig. 7a with peak profiles obtained for longer holding periods.

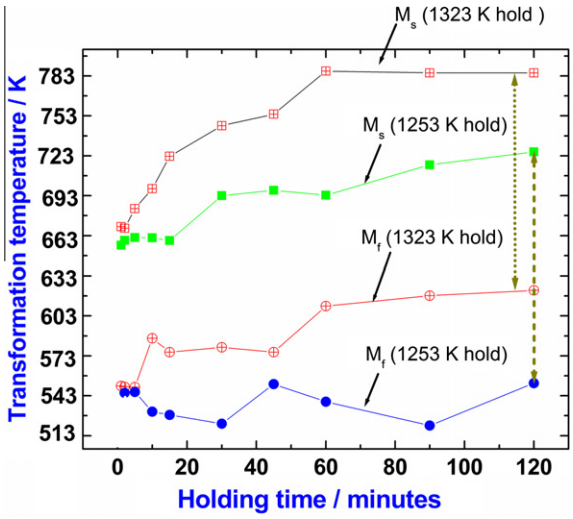

Fig. 8. Variation of M_S and M_f temperatures with holding time at 1253 and 1323 K. The vertical arrows placed at 120 min holding indicate the overall martensitic transformation temperature interval.

corollary of this observation, we may also infer that the nucleation of martensite is seemingly facilitated with increasing holding time in the γ-austenite region. In all probability this may be traced to the effect of austenite grain growth on martensite formation kinetics [77,91]. This will be addressed in detail at a slightly latter point in this section.

In order to study the influence of austenitising temperature on subsequent martensite transformation upon controlled cooling, a similar set of experiments is performed by choosing a slightly higher solutionising temperature of 1323 K. The summary of results obtained is graphically presented in Fig. 8. Two important findings emerge from a careful observation of this figure. At the outset, it is important to note that the top two curves in this figure represent the M_S temperatures for 1323 and 1253 K annealing respectively, while the bottom ones stand for their respective M_f temperatures. The vertical dotted arrows indicate the M_f–M_S temperature gap observed for the largest holding time realised in our experiment, namely 2 h. In the first, it is clear that in the case of 1253 K solutionising treatment, the initial variation of M_S with holding time is rather small; it is only for time periods exceeding about 30 min, a gradual increase in M_S is becoming noticeable. This tendency finally tapers down to reach the saturation behaviour for larger holding times. A somewhat different trend is witnessed in the case of 1323 K solutionising anneal. In this case, a steady increase in M_S with time is noticed right from the early stages of annealing (*see upper curve in* Fig. 8). Therefore, it is clear that the choice of the solutionising temperature plays a crucial role in deciding the initial nucleation and propagation or spreading kinetics of martensite [75–77]. The other important point that emerges from Fig. 8 is that although an increase in the austenitisation temperature from 1253 to 1323 K results in an overall increase of M_S, there is not much of a change in the effective M_f–M_S temperature interval, especially for longer periods of anneal in the γ-austenite domain. This is clearly reflected from the approximately equal length of vertical dotted arrows in Fig. 8. Thus, apart from the initial nucleation aspects of martensite formation, the overall martensite spread kinetics does not seem to be appreciably influenced by a small increase in the austenitisation temperature.

3.4. Carbide dissolution in austenite and its effect on martensite formation

One of the crucial factors that affect austenite grain size, its composition and hence the martensite formation characteristics is the dissolution kinetics of carbides. It is well known that 9Cr-steels depending on minor alloying additions can have both $M_{23}C_6$ and MX type carbides after standard normalising and tempering treatment. Of these, the major $M_{23}C_6$ carbides dissolve at the somewhat lower austenitisation temperatures of 1253–1323 K. Their dissolution kinetics is somewhat sluggish due to slow chromium diffusion. In case of Ta and W containing steels, the diffusivity is expected to be even little lower. On the other hand, the minor MX type carbides containing V and W partly do not dissolve appreciably at 1253–1323 K [86]; however, a little partial dissolution cannot be ruled out, but their completion requires a considerably higher temperature [86]. Therefore, it is expected that the progressive dissolution of carbides during isothermal holds in the austenite phase field may be qualitatively captured in the corresponding DSC traces. These results are displayed in Fig. 9.

Fig. 9 depicts the base line compensated DSC traces observed during various austenitising anneals, that is isothermal holds in the high temperature γ-austenite region. From this figure, we bring out yet another facet of the homogenisation process taking place in RAFM steel. An array of distinctly placed small endothermic peaks is readily evident from these base line compensated DSC profiles.

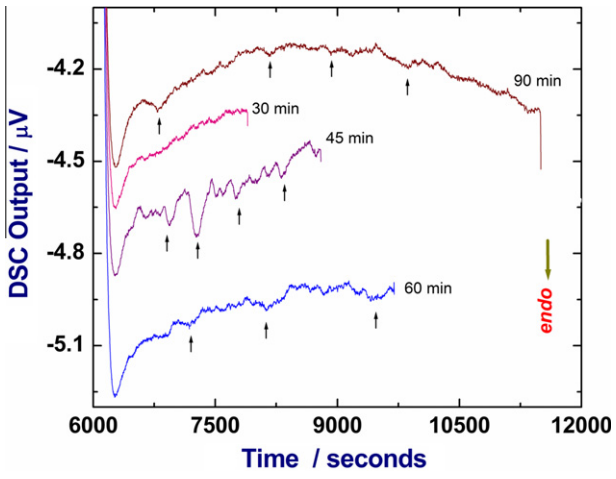

Fig. 9. A stack of baseline compensated isothermal DSC traces recorded at 1253 K indicating small endothermic peaks arising from discrete time dependent carbide dissolution events.

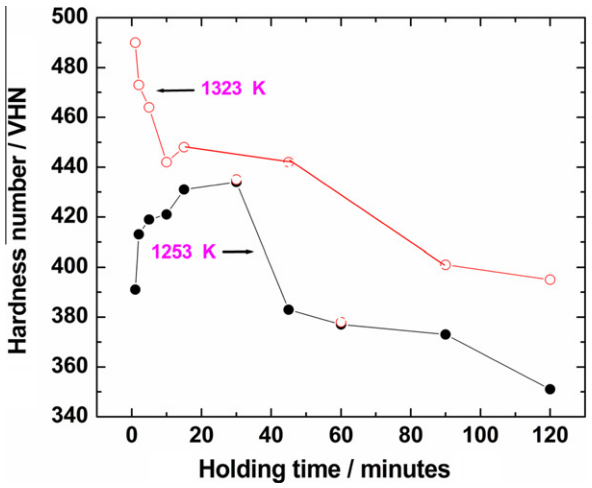

Fig. 10. Variation of martensite hardness with holding time in the austenite region for two different austenitising temperatures, 1253 and 1323 K, respectively.

The first major drop in each signal signifies the default instrumental response due to the onset of an isothermal hold in the experimental schedule. It must be mentioned that although these experiments were conducted with samples of similar size and mass under identical experimental conditions, the distinct attestation of carbide dissolution endothermic events occurred rather discretely in each sample. This behaviour is thus found to be statistical since samples used in different runs are not exactly microstructurally identical with respect to the spatial distribution, size and density of carbide particles. In sample with copious and large carbide particles, the dissolution events were rather more prominent. But what is noteworthy is that even after about 60–90 min of holding at 1253 K, the presence of tiny endothermic wiggles were continued to be observed. Thus, we may infer from Fig. 9 that the process of isothermal austenitisation involves certain well defied time dependent microstructural changes, such as carbide dissolution [92,93], which as the present experimental results suggest, is progressive in nature. Depending on the homogeneity of the starting microstructure at sub-micron level, the carbide dissolution process gets initiated at different time intervals. Subsequently, these events gradually proceed to completion with a time constant that is set by the diffusivity of the slowest of diffusants in this steel. Thus the progressive carbide dissolution produces a net change in the local γ-austenite composition [17,95]. Since the carbide dissolution generally involves a measurable enthalpy change, these are reflected as clearly resolved endothermic peaks or undulations in an otherwise smooth baseline compensated thermal analysis profiles that are expected for reaction free solution annealing. In Fig. 9, the thermal analysis response of isothermal carbide dissolution phenomenon is graphically illustrated, with individual arrow pointers marking well-discernible discrete carbide dissolution events. In particular, the 45 min isothermal hold profile presents nicely delineated carbide dissolution peaks.

A remarkable attestation of the gradual, time dependent carbide dissolution event is also found in the corresponding hardness variation of samples that are quenched (99 K min^{-1}) after the end of different isothermal holds in the γ-austenite regime. This result is graphically portrayed in Fig. 10. The curve at the top depicts the hardness drop as a function of holding time for 1323 K solution annealed samples. The bottom curve represents similar results for 1253 K annealed samples. The adoption of a higher solution anneal temperature namely, 1323 K results in a ready or accelerated dissolution of carbides from the very beginning of the annealing process; in fact the drop in hardness values during the initial part of the curve is rather steep. This dissolution of carbides mostly of $M_{23}C_6$ type enriches the composition of adjacent austenite in chromium and carbon as their solubility in austenite is comparatively large at high temperatures [94]. Since the diffusivity of carbon is comparatively larger than that of the substitutional chromium atoms, the local austenite region surrounding the dissolving carbide will be somewhat rich in chromium [54]. It is this new or nascent chromium rich composition of austenite prevailing at the typical solutionising conditions, which also decides the actual M_S temperature [63,64]. For obvious reasons, a higher chromium content of parent austenite results in an increase of M_S, as Cr is a known ferrite stabiliser.

On the kinetics front, the dissolution of carbides results in the reduction of the pinning effect that these hard particles offer to the unhindered motion of advancing martensite front [78]. On a similar note, one may also observe that the time dependent grain growth in the γ-austenite phase is likewise facilitated as a concomitant or induced effect of carbide dissolution [95,96]. Thus, the adoption of higher solutionising temperature is more effective in promoting the ease of martensite formation on two counts: namely, the enrichment of γ-austenite composition in chromium following carbide dissolution and the kinetic enhancement due to promoted austenite grain growth.

In stark contrast, the *initial* hardness response of martensite produced from 1253 K solution annealed samples first exhibits an increase with annealing time for up to about 30 min and at which point it exhibits the maximal value. This is subsequently followed by a continuous decrease in a manner that is much like the case of 1323 K austenitised samples. Obviously, this difference in the initial response of the hardness curve between these two annealing temperatures stems from the sluggish nature of carbide dissolution step at 1253 K [92,93]. For smaller time holds at 1253 K, the parent austenite phase still contains quite an extent of undissolved carbides as compared to 1323 K. Further, the lack of carbide dissolution means that the austenite is not getting that much enriched in chromium which is a known ferrite stabiliser. Both these facts act together to give a transformation product with lower M_S temperature and which also contains some undissolved carbide (Fig. 8). The higher hardness is from the composite presence of carbides present in quenched in martensite. The lower M_S temperature is from the relatively low chromium content of the parent austenite. Unlike in low alloy steels, where the carbide dissolution kinetics is known to be fairly rapid [97], the kinetics of

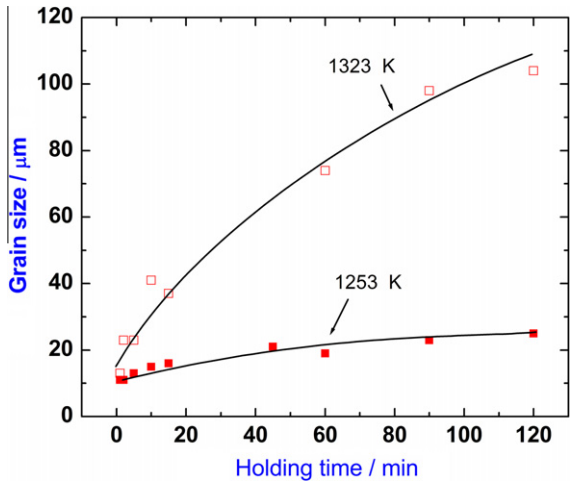

Fig. 11. Variation of austenite grain size with holding time at 1253 and 1323 K, respectively.

austenite formation and carbide dissolution in highly alloyed low to moderate carbon steels has been reported to be much sluggish, as the classical studies of Lenel and Honeycombe and that of Shtansky et al., suggest [92–94]. Moreover, the slow carbide dissolution kinetics which is compounded by the sluggish transportation of the dissolved chromium away from the carbide/matrix interface into the bulk causes appreciable solute build up near the reaction front, which could also manifests as a sort of solute drag effect on the overall solutionising kinetics. Thus, the kinetics of α-ferrite + carbides → γ-austenite transformation which is taking place in the high temperature austenite domain during homogenisation treatment is crucially dependent on the choice of the austenitising temperature, in addition to time.

As an additional point, we may also add that measurement of parent γ-austenite grain size has been made as a function holding time for both 1323 K and 1253 K solution annealed samples. These results are displayed in Fig. 11. From this figure, it is clearly seen that the adoption of a slightly higher annealing temperature of 1323 K promotes grain growth in austenite to a much greater extent. It is in order to avoid this excessive grain growth, a relatively low normalising temperature of about 1253 K is chosen for present RAFM. As stated before, an enquiry into the mechanistic aspects of austenite grain growth must take into account the concurrent occurrence of carbide dissolution and thereby the reduction in their pinning potential of the growing austenite grain boundaries against the intrinsic interface energy driven grain coarsening tendency [96]. Since the present discussion is oriented more towards the elucidation of martensite formation based on calorimetry experiments, a detailed discussion of austenite grain growth kinetics is not taken up here.

4. Discussion

4.1. General remarks

Although the field of martensitic transformation, especially in ferrous alloy systems has been an extensively researched one, the application of calorimetric techniques to elucidate its kinetic characteristics has not been that extensively pursued, as compared to microscopy or dilatometry, for example. To the best of the author's knowledge, there were relatively few studies devoted exclusively to measuring the martensite transformation kinetics as a function of composition, grain size, cooling rate etc., in ferrous alloys using calorimetry [26,90]. In the case of reduced activation steels meant for fusion reactor applications, such studies were even fewer. It must be added that careful calorimetry measurements are a boon for obtaining vital thermodynamic and kinetic data on martensitic transformation. These data are of immense value in thermodynamic modelling of martensitic phase transformations in general [97–109]. It is amidst this backdrop, the theme of the present study has been framed. In what follows, we present a brief discussion of the major findings of our study in the light of the currently held viewpoints on athermal martensite formation in Fe-based alloys.

4.2. Enthalpy of martensite formation, M_S temperature and grain size effect

The M_S and M_f temperatures obtained in this study for the RAFM steel are 714 and 614 K respectively. Since M_S is as much a kinetic quantity as it is thermodynamic in origin, the present values are slightly sensitive to the specifics of the heat treatment, besides actual austenite composition at the austenitisation temperature [89,97]. Notwithstanding such a caveat, the measured values are found to be in fair degree of agreement with the reported values for 9Cr-based low carbon power plant steels [42,90]. The enthalpy for the γ → α'– martensite transformation $\Delta^{\circ}H^{\gamma\rightarrow\alpha'}$, as estimated from the measured transformation peak area after appropriate calibration is found to be in the range 64–75 J g^{-1}. There are not many recent estimates of this quantity in the metallurgical literature, almost none for advanced nuclear power plant steels [90]. Therefore the present discussion derives heavily from some of the classical calorimetry studies.

In a classical study using isoperibol type drop calorimeter, Lee et al. have measured martensite formation enthalpy for some Fe–Ni, Fe–Ni–Mn, Fe–Ni–C, Fe–Ni–Cr–C stainless steel alloys [108]. They found that $\Delta^{\circ}H^{\gamma\rightarrow\alpha'}$, in addition to deriving a contribution from composition, is also substantially influenced by the nature of martensite substructure. Thus for example, a twin martensite with a higher amount of stored energy is found to possess relatively lower transformation enthalpy than the dislocation laden lath type martensite. This difference is attributed to the increased stored energy in case of twin marteniste, which is not released as a part of the transformation heat during phase change [108]. The reason for bringing this fact into present discussion is to stress the viewpoint that the enthalpy effects as detected by calorimetry for a nonequilibrium phase change like martensite formation is generally subject to a larger degree of scatter, which *per se* is intrinsic to the nature of phase change, in addition to the limitations of the sensing technique. As shown in Fig. 1b, the martensite in RAFM is basically of lath type with high dislocation density. In this light, the present experimental estimate 64–75 J g^{-1} for the transformation enthalpy is expected to be a little high by virtue of the large amount of stored energy. In a sense, this also borne out by our earlier DSC based measurement of the specific heat of martensite [86]. In their study on Fe–1.9Cr–.53Mn–.6C–.02Si–.02Co (wt.%) alloy, Lee et al. obtain an estimate of 2740 J mol^{-1} for $\Delta^{\circ}H^{\gamma\rightarrow\alpha'}$, the net martensite transformation enthalpy estimated at 510 K [108]. This is lath martensite with a different composition from our RAFM steel. Assuming an average atomic weight of about 55 for the present RAFM steel, the present experimental estimates for $\Delta^{\circ}H^{\gamma\rightarrow\alpha'}$ translate to 3520–4125 J mol^{-1}. If a stored energy contribution of 1400 J mol^{-1}, which is typical of lath martensites is discounted from this total value [108], we then get a value in the range 2725–2120 J mol^{-1} for the chemical contribution to the overall martensite transformation enthalpy of RAFM steel. This estimated value for the formation of hypothetical strain free martensite is certainly greater than the experimental enthalpy obtained for the diffusional on-heating α-ferrite + carbide → γ-austenite transformation [86]. Thus in a nutshell, the microstructure or strain contribution to martensite transformation is quite

appreciable for highly alloyed ferrous martensites and this is also supported by present findings. But we hasten to add that more experimental work on many controlled alloy compositions is needed to throw further insight on this interesting basic issue.

4.3. Critical cooling rate, carbide dissolution and grain size effect

In the present study, the critical cooling rate to form nearly 100 percent martensite is found to be of the order of 5–6 K min^{-1}, for the 1253 K normalising treatment. This value is slightly higher than the corresponding estimate of about 1 K min^{-1} reported for modified 9Cr-steel [86]. As discussed in the previous section, M_S is essentially decided by the austenite composition prevailing at the solutionising temperature. In addition, it is also dependent on austenite grain size and the presence of any external stress [89,103]. Ignoring the influence of stress in the present discussion, it emerges from the results obtained here, that both the effective austenite composition and its grain size are the two deciding factors and these are controlled by the austenitisation temperature and time.

To begin with, it is instructive to recall that RAFM steel is almost free of Mo and Nb, which are invariably present in a typical modified 9Cr-steel composition, such as P91 or T91. The substitution of these elements by more cohesive *bcc* neighbours like W and Ta raises in general all the diffusive transformation temperatures, which include $M_{23}C_6$, MX carbide dissolution solvii, the temperature of austenite and δ-ferrite formation, etc. [86]. The major effect of the increased cohesion brought about by W and Ta addition is that for a relatively low normalising temperature of 1253 K adopted in this study, the carbide dissolution is never realised to its completion in the usually adopted solutionising time of about 30 min. This is found to be true even with our *small specimen* studies, in which almost nil or only a minimal thermal gradient is expected across the entire cross section. A CALPHAD simulation done using ThermoCalc software and critically assessed multicomponent thermodynamic database for Fe-based systems, also suggests higher solution temperatures for W and Ta containing carbides that are encountered in this steel [49,50]. Therefore, it is clear that for most part of the time during shallow austenitisation anneal, there will be a definite presence of some undissolved carbides, which are quite conducive to restraining the growth of austenite grains through the mechanism of Zener pinning [110]. In addition, the sluggish carbide dissolution would not serve to enrich the austenite composition in Cr, Ta and W, if the solution anneal were to be carried out at lower temperatures in the γ-austenite phase field. The net effect in such a situation is the achievement of relatively small austenite grain sizes (Fig. 11) with not much change in γ-austenite composition from the starting base composition.

Since athermal martensite nucleation is known to be heterogeneous in nature [102,105], and further the austenite grain boundaries are not known to serve as potential nucleating sites for martensite [77], the fine grained austenite do not necessarily promote martensite transformation [91,111]. Since martensite propagation in ferrous alloys is one of mainly through bursts, the austenite grain boundaries only serve to impede the growth of martensite plates. A larger austenite grain size on the other hand facilitates laths of larger linear dimensions which by virtue of the strain field at its tips serve to nucleate another cluster in a neighbouring grain [75–77]. Thus from kinetics point of view, larger austenite grain size promotes martensite nucleation and growth. In Fig. 12, the present experimental findings of grain size effect on M_S temperature is graphically summarised.

In the light of this simple picture, it is now clear as to why the M_S and M_f temperatures are relatively depressed for 1253 K normalised samples. It is also interesting to note that the prior austenite grain sizes enclosing the martensite colony are also small in this case (Figs. 11 and 12), which is why this annealing temperature is selected for the RAFM steel. The adoption of 1323 K as the anneal-

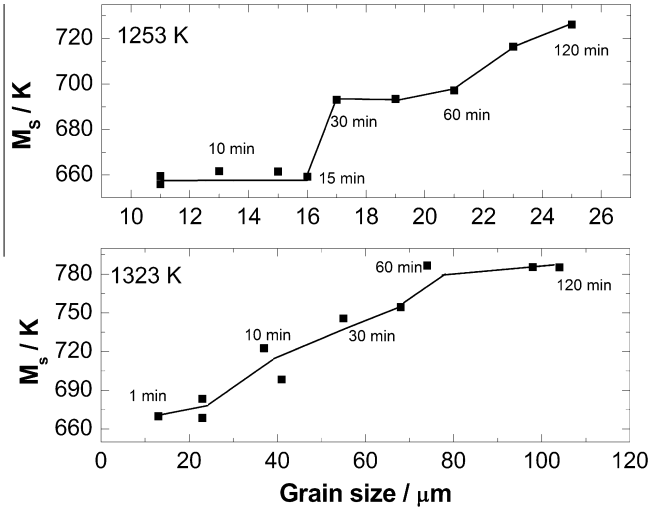

Fig. 12. Variation of M_S temperature with austenite grain size at 1253 and 1323 K, respectively.

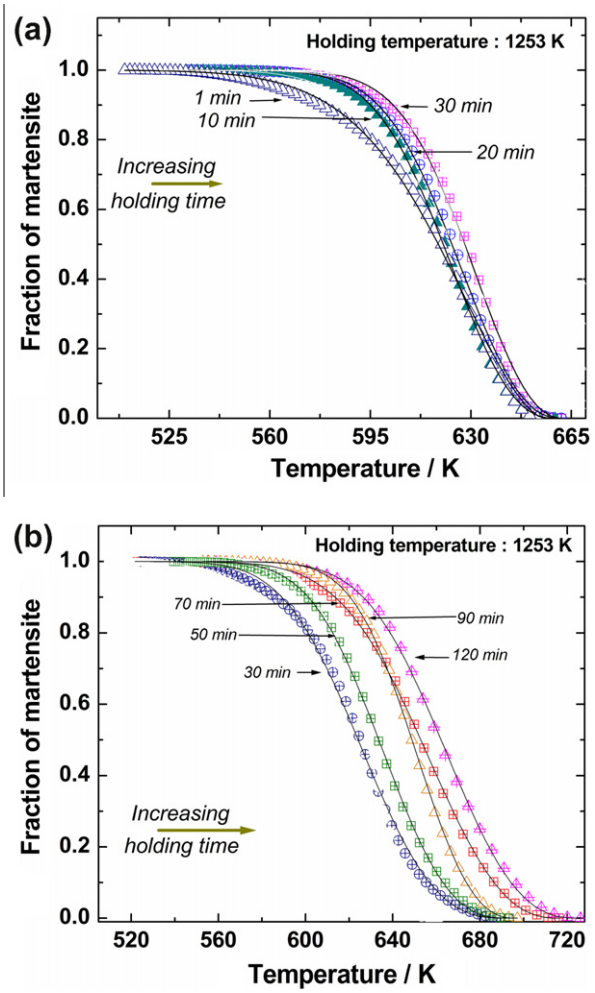

Fig. 13. Fraction of martensite formed as a function of undercooling below M_S for samples that are subject to austenitisation treatment at 1253 K for: (a) 1–30 min and (b) 30–120 min. The line through the curves represents the Koistinen–Marburger fit (Eq. (2)) to the transformation data.

Table 2
Listing of the parameters of the Koistinen–Marburger fit (Eq. (2)) to the experimental data.

Holding time at 1253 K (min)	M_S (K)	M_f (K)	C	n	R^2 value
1	656	508	0.03752 ± 0.00011	1.71145 ± 0.01343	0.99777
2	660	545	0.04342 ± 0.00007	2.14442 ± 0.01005	0.99956
5	662	546	0.04087 ± 0.00012	2.18828 ± 0.01966	0.99839
10	662	531	0.03702 ± 0.00006	2.32103 ± 0.01306	0.99936
15	659	528	0.03636 ± 0.00006	2.39268 ± 0.0136	0.99935
30	693	522	0.02109 ± 0.00004	2.92995 ± 0.0229	0.99862
45	697	551	0.02962 ± 0.00004	2.60108 ± 0.01118	0.9997
60	694	538	0.02415 ± 0.00003	2.78195 ± 0.01154	0.99971
90	716	522	0.02243 ± 0.00003	2.49416 ± 0.01137	0.99961
120	726	553	0.02253 ± 0.02253	2.70304 ± 0.0175	0.99943

ing temperature on the contrary promotes rapid grain growth, which serves to increase the M_S and M_f temperatures (Fig. 12), but results in a reduction of its strength, as reflected by the drop in hardness (Fig. 10).

4.4. Martensitic transformation kinetics

In Fig. 13a and b, the fraction of martensite formed as a function of temperature is plotted for different samples that have undergone different extents of austenitisation at 1253 K. For reasons of space and brevity, only results pertaining 1253 K austenitising treatment are discussed here. It must be added that all these samples are cooled at a uniform rate of 99 K min^{-1} to room temperature. Assuming that the total area under the transformation peak corresponds to 100 percent martensite formation, the fraction transformed at any intermediate temperature T, such that $M_S < T < M_f$, can be estimated from the following relation.

$$f(T) = \left[\int_{M_S}^{T} \phi dT\right] / \left[\int_{M_S}^{M_f} \phi dT\right] \quad (1)$$

The integral in the numerator stands for the partial peak area measured in the temperature range M_S to T, while that in the denominator stands for the full peak area spanning from M_f to M_S. The discrete points in Fig. 13 denote the actual experimental data obtained using Eq. (1), while the continuous line passing through them represents the Koistinen–Marburger (K–M) fit given by the expression [112].

$$f'_\alpha = 1 - \exp[C/\beta(M_S - T)]^n \quad (2)$$

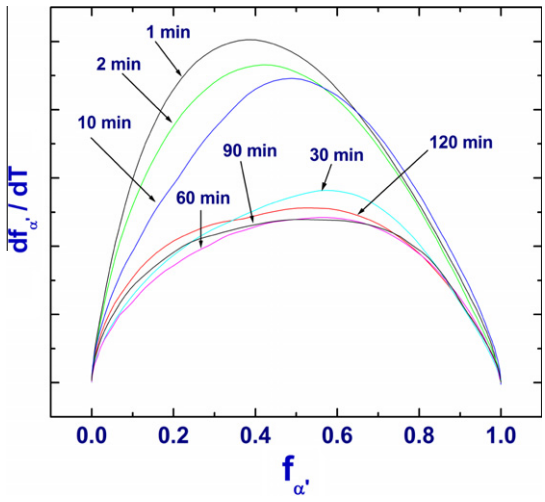

Fig. 14. The rate of martensite formation is plotted as a function of martensite fraction for samples that are solution treated at 1253 K for different durations.

In Eq. (2), $f_{\alpha'}(T)$ is the fraction of martensite formed as a function of temperature T, below M_S, C is an empirical rate constant and n is the transformation exponent, again assumed in the empirical sense. In order to incorporate the cooling rate effect in Koistinen–Marburger relation, Eq. (2) is written in a modified form by absorbing in the prefactor the cooling rate β in an explicit manner [113]. As judged from Fig. 13, the K–M relation fits the present experimental data rather well and the fit parameters are listed in Table 2. It emerges from Fig. 13a, that for holding times up to about 30 min, the different transformation curves are closely overlapping, suggesting thereby that martensite transformation kinetics is not very much differentiated in this regime. The average value of C/β as listed in Table 2 turns out to be about 0.001, which incidentally agrees well with the original proposition of Koistinen–Marburger [112].

In Fig. 14, another interesting manifestation of the holding time effect on martensitic transformation kinetics is illustrated. It emerges from this figure that in samples which had seen only smaller durations of austenitising anneal, the maximum in the rate of martensite formation, that is the quantity $df_{\alpha'}/dT$ is realised at a value of about 0.2–0.4 for f_α, the fraction of martensite formed. However for longer anneals, which is synonymous with larger austenite grain size, the maximum transformation rate is realised at $f_\alpha \sim 0.6$. This is again supportive of the deduction that austenite grain growth catalyses martensite spread kinetics.

5. Conclusions

(i) A comprehensive characterisation of the kinetics of martensitic transformation phenomenon in RAFM s has been carried out using differential scanning calorimetry. The effects of holding temperature and time in the γ-austenite phase field and also the cooling rate on the martensite start temperature M_S have been precisely quantified.

(ii) The M_S and M_f temperatures for 1253 K/15 min normalised samples are found to be 714 and 614 K respectively. The transformation enthalpy for martensite formation is estimated to be 64–75 J g^{-1}. The critical cooling rate for the austenitisation temperature 1253 K is found to between 5 and 6 K min^{-1}.

(iii) The M_S temperature exhibited a continuous increase with increasing holding times for 1323 K austenitisation treatment. The corresponding martensite hardness values exhibited a systematic drop. In case of 1253 K austenitisation anneal, the M_S temperature did not evince much of a change with holding time for the initial region. However, for annealing periods exceeding 30 min, the M_S has started showing a steady increase. For both 1253 and 1323 K austenitisation anneals, the martesnitic transformation interval M_f–M_S, do not exhibit any substantial difference for the longer annealing periods.

(iv) The large prior austenite grain size which is obtained for longer annealing durations is found to promote the kinetics of martensite formation. The slow carbide dissolution phenomenon which co-occurs during the initial phase of annealing at lower solutionising temperature is found to have an indirect influence on M_S temperature, by slowing down the austenite grain coarsening.

(v) The kinetics of martensite formation is found to follow the empirical Koistinen–Marburger relation.

Acknowledgements

The authors gratefully acknowledge the encouragement and sustained support that they have received from Dr. T. Jayakumar and Dr. M. Vijayalakshmi, during the course of this research. The experimental assistance received from Miss. P. Brindha, – an M. Phil., research scholar during the formative phase of this research is sincerely acknowledged. As a token of our respect, this paper is dedicated to the fond memories of Prof. P. Ramachandra Rao.

References

[1] Fujio Abe, Sci. Technol. Adv. Mater. 9 (2008) 1–15.
[2] H.K.D.H. Bhadeshia, ISIJ Int. 41 (2001) 626–640.
[3] Fujimitsu Masuyama, ISIJ Int. 41 (2001) 612–625.
[4] Ulrich E. Klotz, Christian Solenthaler, D.J. Uggowitzer, Mater. Sci. Eng. A76 (2008) 186–194.
[5] H. Cerjak, P. Hofer, B. Schaffernak, ISIJ Int. 39 (1999) 874–888.
[6] J.W. Morris Jr., Z. Guo, C.R. Krenn, Y.-H. Kim, ISIJ Int. 41 (2001) 599–611.
[7] J.M. Vitek, R.L. Klueh, Metall. Trans. A 14A (1983) 1047–1055.
[8] J. Hald, Int. J. Press. Vessel Piping 85 (2008) 30–37.
[9] G. Krauss, ISIJ Int. 35 (1995) 349–359.
[10] V. Knezevic, G. Sauthoff, J. Vilk, G. Inden, A. Schneider, R. Agamennone, W. Blum, Y. Wang, A. Scholz, C. Berger, J. Ehlers, L. Singheiser, ISIJ Int. 42 (2002) 1505–1514.
[11] V. Thomas Paul, S. Saroja, M. Vijayalakshmi, J. Nucl. Mater. 378 (2008) 273–281.
[12] M. Igarashi, S. Muneki, H. Hasegawa, K. Yamada, F. Abe, ISIJ Int. 41 (Suppl.) (2001) S101–S105.
[13] X.Y. Liu, T. Fujita, ISIJ Int. 29 (1989) 680–686.
[14] M. Tamura, H. Kusuyama. Kei Shinozuka, H. Esaka, ISIJ Int. 47 (2007) 317–326.
[15] K. Maile, Int. J. Press. Vessel Piping 84 (2007) 62–68.
[16] F. Abe, M. Tabuchi, M. Kondo, S. Tsukamoto, Int. J. Press. Vessel Piping 84 (2007) 44–52.
[17] L.F. Alvarez, C. Garcia, V. Lopez, ISIJ Int. 34 (1994) 516–521.
[18] P. Hofer, M.K. Miller, S.S. Babu, S.A. David, H.A. Cerjak, ISIJ Int. 42 (Suppl.) (2002) S62–S66.
[19] T. Hasegawa, Y.R. Abe, Y. Tomita, N. Maruyama, M. Sugiyama, ISIJ Int. 41 (2001) 922–929.
[20] M. Tamura, H. Hayakawa, A. Yoshitake, A. Hishinuma, T. Kondo, J. Nucl. Mater. 155–157 (1988) 620–625.
[21] R. Kishore, R.N. Singh, T.K. Sinha, B.P. Kashyap, J. Nucl. Mater. 195 (1992) 198–204.
[22] M. Tamura, H. Iida, H. Esaka, K. Shinozuka, ISIJ Int. 43 (2003) 1807–1813.
[23] S.G. Hong, W.B. Lee, C.G. Park, Scripta Mater. 43 (2000) 181–196.
[24] S.G. Hong, W.B. Lee, C.G. Park, J. Nucl. Mater. 288 (2001) 202–207.
[25] F. Abe, T. Noda, H. Araki, S. Nakazawa, J. Nucl. Mater. 179–181 (1991) 663–666.
[26] S. Raju, B. Beyaganesh, A. Banerjee, E. Mohandas, Mater. Sci. Eng. A465 (2007) 29–37.
[27] F. Abe, T. Horiuchi, M. Taneike, K. Sawada, Mater. Sci. Eng. A378 (2004) 299–303.
[28] A. Zielinska-Lipiec, A. Czyrska-Filemonowicz, P.J. Ennis, O. Watcher, J. Mater. Proc. Technol. 64 (1997) 397–405.
[29] K. Kaneko, S. Matsuyama, A. Sadakata, K. Fujita, W.J. Moon, S. Ozaki, N. Nishimura, Y. Tomokiyo, Mater. Sci. Eng. A374 (2004) 82–89.
[30] K. Yamada, M. Igarashi, S. Muneki, F. Abe, ISIJ Int. 42 (2002) 779–784.
[31] F. Abe, Mater. Sci. Eng. A319–321 (2001) 770–773.
[32] K. Yamada, M. Igarashi, S. Muneki, F. Abe, ISIJ Int. 41 (Suppl.) (2001) S116–S120.
[33] M. Tamura, Y. Haruguchi, M. Yamashita, Y. Nagaoka, K. Ohinata, K. Ohnishi, E. Itoh, H. Ito, K. Shinozuka, H. Esaka, ISIJ Int. 46 (2006) 1693–1702.
[34] Y. Murata, M. Kamiya, T. Kuneida, A.M. Abdel-Daiem, T. Koyama, M. Morinaga, R. Hashizume, ISIJ Int. 45 (2005) 101–105.
[35] K. Iwanaga, T. Tsuchiyama, S. Takai, Key Eng. Mater. 171–174 (2000) 477–482.
[36] T.K. Kim, J.H. Baek, C.H. Han, S.K. Kim, C.B. Lee, J. Nucl. Mater. 389 (2009) 359–364.
[37] R. Jayaram, R.L. Klueh, Metall. Mater. Trans. 29A (1998) 1551–1558.
[38] J.M. Koo, S.Y. Kim, K. Shin, Y.G. Jung, S.K. Hur, Key Eng. Mater. 345–346 (2007) 465–468.
[39] V. Homolova, J. Janovec, P. Zahumensky, A. Vyrostkova, Mater. Sci. Eng. A 349 (2003) 306–312.
[40] M. Yoshino, Y. Mishima, Y. Toda, H. Kushima, K. Sawada, K. Kimura, ISIJ Int. 45 (2005) 107–115.
[41] K. Sawada, T. Ohba, H. Kushima, K. Kimura, Mater. Sci. Eng. A394 (2005) 36–42.
[42] H. Finkler, M. Schirra, Steel Res. 67 (1996) 328–342.
[43] Y. Tsuchida, K. Okamoto, Y. Tokunaka, ISIJ Int. 35 (1995) 317–323.
[44] H.D. Kim, I.S. Kim, ISIJ Int. 34 (1994) 198–204.
[45] V. Foldyna, J. Purmensky, Z. Kuban, ISIJ Int. 41 (2001) S81–S85.
[46] V. Fodarek, A. Strang, Mater. Sci. Technol. 16 (2000) 1207–1213.
[47] S. Kobayashi, K. Toshimori, K. Nakai, Y. Ohmori, H. Asahi, T. Muraki, ISIJ Int. 42 (2002) S72–S76.
[48] K. Maruyama, K. Sawada, ISIJ Int. 41 (2001) 641–653.
[49] A. Danon, C. Servant, J. Nucl. Mater. 321 (2003) 8–18.
[50] A. Danon, C. Servant, ISIJ Int. 45 (2005) 903–912.
[51] J.-O. Andersson, Metall. Trans. 14A (1988) 627–636.
[52] V.A. Yardley, Y. De Carlan, J. Phase Equilib. Diffuse. 27 (2006) 102–112.
[53] A. Kroupa, J. Havrankova, M. Coufalova, M. Svoboda, J. Vrestal, J. Phase Equilib. Diffuse. 22 (2001) 312–323.
[54] A. Bjarbo, M. Hatterstrand, Metall. Trans. 32A (2001) 19–27.
[55] B.C. Schaffernak, H. Cerjak, Calphad 25 (2001) 241–251.
[56] J.D. Robson, H.K.D.H. Bhadeshia, Calphad 20 (1996) 447–460.
[57] F.G. Caballero, C. Capdevila, C. Garcia de Anders, ISIJ Int. 41 (2001) 1093–1102.
[58] A. Schneider, G. Inden, Acta Mater. 53 (2005) 519–531.
[59] R.G. Thiessen, I.M. Richardson, J. Sietsma, Mater. Sci. Eng. A427 (2006) 223–231.
[60] M. Perez, A. Deschamps, Mater. Sci. Eng. A360 (2003) 214–219.
[61] M. Sob, A. Kroupa, J. Pavlu, J. Vrestal, Solid State. Phenomena 150 (2009) 1–28.
[62] Y. Murata, T. Koyama, M. Morinaga, T. Miyazaki, ISIJ Int. 42 (2002) 1423–1429.
[63] T. Sourmail, C. Garcia-Mateo, Comput. Mater. Sci. 34 (2005) 323–334.
[64] T. Cool, H.K.D.H. Bhadeshia, Mater. Sci. Technol. 12 (1996) 40–44.
[65] L. Gavard, H.K.D.H. Bhadeshia, D.J.C. MacKay, S. Suzuki, Mater. Sci. Technol. 12 (1996) 453–463.
[66] Q. Li, Mater. Sci. Eng. A361 (2003) 385–391.
[67] R.G. Faulkner, Acta Metall. 35 (1987) 2905–2914.
[68] You Ya Fin, R.G. Faulkner, Mater. Sci. Eng. A344 (2003) 92–102.
[69] P. Maugis, D. Gendt, S. Lanteri, P. Barges, Defect. Diffuse Forum 194–199 (2001) 1767–1772.
[70] J. Miettinen, Calphad 22 (1988) 275–300.
[71] F. Masuyama, Mater. Sci. Eng. A510–511 (2009) 158–161.
[72] M.Y. He, G.R. Odette, T. Yamamoto, D. Klingensmith, J. Nucl. Mater. 367–370 (2007) 556–560.
[73] C. Kocer, T. Abe, A. Soon, Mater. Sci. Eng. A505 (2009) 1–5.
[74] J. Agren, ISIJ Int. 32 (1992) 291–296.
[75] J.R.C. Guimaraes, A. Saavedra, Mater. Sci. Eng. 62 (1984) 11–15.
[76] J.R.C. Guimaraes, Mater. Sci. Eng. A476 (2008) 106–111.
[77] J.R.C. Guimaraes, J.C. Gomez, Acta Metall. 26 (1978) 1591–1596.
[78] S. Kustov, J. Pons, E. Cesari, J. Van Humbeeck, Acta Mater. 52 (2004) 3075–3081.
[79] D. Gaude-Fugarolas, Y. de Carlan, J. Nucl. Mater. 374 (2008) 109–115.
[80] J.-B. Leblond, G. Mottet, J. Devaux, J.-C. Devaux, Mater. Sci. Technol. 1 (1985) 815–822.
[81] J. Agren, Scand. J. Metall. 19 (1990) 2–8.
[82] S.G.E. teVelthuis, N.H. Van Dijk, M. Th. Rekveldt, J. Sietsma, S. Van der Zwaag, Mater. Sci. Eng. A277 (2000) 218–228.
[83] S. Denis, D. Farias, A. Simon, ISIJ Int. 32 (1992) 316–325.
[84] W. Xu, Mater. Sci. Eng. A467 (2007) 24–32.
[85] S. Sharafat, G.R. Odette, J. Blanchard, J. Nucl. Mater. 386–388 (2009) 896–899.
[86] S. Raju, B. Jeyaganesh, A.K. Rai, R. Mythili, S. Saroja, E. Mohandas, M. Vijayalakshmi, K.B.S. Rao, Baldev Raj, J. Nucl. Mater. 389 (2009) 385–393.
[87] R.L. Klueh, Int. Mater. Rev. 50 (2005) 287–310.
[88] R. Lindau, A. Moslang, M. Schirra, Fusion Eng. Design 61–62 (2002) 659–664.
[89] E. Hornbogen, Acta Metall. 33 (1985) 595–601.
[90] B. Jeyaganesh, S. Raju, A. K. Rai, R. Mythili, E. Mohandas, M. Vijayalakshmi, K. B. S. Rao, Baldev Raj, Mater. Sci. Technol. (2010) in press..
[91] A. Garcia Junceda, C. Capdevila, F.G. Caballero, C. Garcia de Andres, Scripta Mater. 58 (2008) 134–137.
[92] U.R. Lenel, R.W.K. Honeycombe, Metal Sci. 18 (1984) 201–205.
[93] U.R. Lenel, Scripta Metall. 17 (1983) 471–476.
[94] D.V. Shtansky, G. Inden, Acta Mater. 45 (1997) 2879–2895.
[95] A. Danon, C. Servant, A. Alamo, J.C. Brachet, Mater. Sci. Eng. A348 (2003) 122–132.
[96] M. Shome, D.S. Sarma, O.P. Gupta, O.N. Mohanty, ISIJ Int. 43 (2003) 1431–1437.
[97] M. Palumbo, Calphad 32 (2008) 693–708.
[98] G.N. Haidemenopoulos, M. Grujicic, G.B. Olson, M. Cohen, J. Alloys Compos. 220 (1995) 142–147.
[99] G.N. Haidemenipoulos, A.N. Vasilakos, J. Alloys Compos. 247 (1997) 128–133.

[100] Zhao Jicheng, Acta Metall. Mater. 38 (1990) 425–431.
[101] J. Kunze, B. Beyer, Z. Metallkd. 91 (2000) 10–16.
[102] A. Borgenstam, M. Hillert, Acta Mater. 45 (1997) 2079–2091.
[103] H. Kato, S. Miura, Acta Metall. Mater. 43 (1995) 351–360.
[104] P. Wollants, M. De Bonte, J.R. Roos, Z. Metallkd. 70 (1979) 113–117.
[105] G. Ghosh, G.B. Olson, Acta Metall. Mater. 42 (1994) 3361–3370.
[106] G. Ghosh, G.B. Olson, Acta Metall. Mater. 42 (1994) 3371–3379.
[107] J. Kunze, B. Beyer, Z. Metallkd. 91 (2000) 106–113.
[108] B. Lee, S. Millman, I.L. MacDougall, S.R. Keown, B.B. Argent, Metal Sci. 11 (1977) 261–271.
[109] A. Paul, A. Beirante, N. Franco, E. Alves, J.A. Odrizolo, Mater. Sci. Forum 514–516 (2006) 500–504.
[110] C.R. Hutchinson, H.S. Zurob, C.W. Sinclair, Y.J.M. Brechet, Scripta Mater. 59 (2008) 635–637.
[111] J.R.C. Guimaraes, Scripta Mater. 57 (2007) 237–239.
[112] D.P. Koistinen, R.E. Marburger, Acta Metall. 7 (1959) 59–60.
[113] A.K. Rai, S. Raju, B. Jeyaganesh, E. Mohandas, S. Sudha, V. Ganesan, J. Nucl. Mater. 383 (2009) 215–225.